Link alla cartella GitHub:

https://github.com/alessandragranata/Homwork$_{4F}SR.git$

Università degli Studi di Napoli Federico II

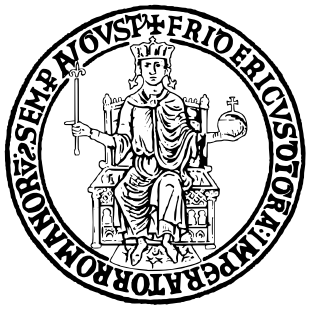

Scuola Politecnica e delle Scienze di Base

Dipartimento di Ingegneria Elettrica e Tecnologie dell'Informazione

Corso di Laurea Magistrale in Automazione e Robotica

Fields and Service Robotics

Homework 4

Relatore
Prof. Fabio Ruggiero

Candidata
Alessandra Granata P38000279

Anno Accademico 2024–2025

1. Buoyancy effect

Buoyancy is a hydrostatic force that acts in the opposite direction to gravity when a body is submerged in a fluid. It does not depend on the relative motion between the body and the fluid, but solely on the static properties of the system. It is proportional to the volume of the submerged body, the density of the fluid, and the gravitational acceleration, according to the following relation:

$$\mathbf{b} = \rho \Delta \, \|\bar{\mathbf{g}}\|$$

where: $\rho \in \mathbb{R}$ is the fluid density, $\Delta \in \mathbb{R}$ is the volume of the submerged body, and $\|\bar{\mathbf{g}}\|$ is the norm of the gravity vector, with

$$\bar{\mathbf{g}} = \begin{bmatrix} 0 \\ 0 \\ g \end{bmatrix} \in \mathbb{R}^3, \quad g \in \mathbb{R} \text{ (gravitational acceleration)}.$$

The submerged weight of the body is instead given by:

$$w = m \, \|\bar{\mathbf{g}}\|$$

where $m \in \mathbb{R}$ is the mass of the body.
In **underwater robotics**, this effect cannot be neglected, because the density of water is comparable to the density of the robot's body. Under these conditions, the buoyancy force may have a magnitude similar to or greater than the robot's weight, allowing it to float, sink, or maintain hydrostatic equilibrium at a certain depth. This condition depends on the geometry of the body and the distribution of its mass. A critical aspect is that the gravitational force is applied at the center of mass of the robot, denoted as $\mathbf{r}_c^b \in \mathbb{R}^3$, and it is modeled in the body-fixed frame as:

$$\mathbf{f}_g^b = \mathbf{R}_b^\top \begin{bmatrix} 0 \\ 0 \\ w \end{bmatrix} = \mathbf{R}_b^\top \begin{bmatrix} 0 \\ 0 \\ mg \end{bmatrix}$$

Meanwhile, the buoyancy force acts at the center of buoyancy, denoted as $\mathbf{r}_b^b \in \mathbb{R}^3$, which does not necessarily coincide with the center of mass, and it is expressed as:

$$\mathbf{f}_b^b = -\mathbf{R}_b^\top \begin{bmatrix} 0 \\ 0 \\ b \end{bmatrix} = -\mathbf{R}_b^\top \begin{bmatrix} 0 \\ 0 \\ \rho \Delta \, g \end{bmatrix}$$

This non-coincidence between the application points of the two forces can generate undesired torques around the robot's body. In fact, in the complete dynamic model, the *wrench* resulting from gravity and buoyancy in the body-fixed frame is given by:

$$\mathbf{g}_{rb}^b = \begin{bmatrix} \mathbf{f}_g^b + \mathbf{f}_b^b \\ \mathcal{S}(\mathbf{r}_c^b)\, \mathbf{f}_g^b + \mathcal{S}(\mathbf{r}_b^b)\, \mathbf{f}_b^b \end{bmatrix} \in \mathbb{R}^6$$

where $\mathcal{S}(\cdot)$ denotes the *skew-symmetric operator* associated with the vector cross product.
In practice, to avoid destabilizing effects, underwater vehicles are often designed so that the center of mass and the center of buoyancy are vertically aligned. In this case, the two forces act along the same vertical line, but in opposite directions, preventing the generation of torques that might affect the robot's attitude, especially during depth changes or tilting maneuvers.
By contrast, in **aerial robotics**, the buoyancy force is completely neglected. This is because air has a much lower density than the materials used to construct flying robots. Although the physical principle is the same, in practice the buoyant force is several orders of magnitude smaller than the gravitational force and does not significantly affect the system dynamics.
In conclusion, buoyancy is explicitly modeled in underwater robotics because it has a fundamental impact on the equilibrium and stability of the vehicle. In contrast, in aerial robotics, it is ignored, as it is practically negligible compared to other relevant dynamic terms.

2. True or False Statements on Hydrodynamic Effects in Underwater Robotics

a. The added mass effect considers an additional load to the structure. **FALSE.**
When a body moves or accelerates within a fluid, it is not only displacing itself but also a portion of the surrounding fluid, which gets dragged and accelerated. This generates *reaction forces* exerted by the fluid on the body, equal in magnitude and opposite in direction to the force the body applies to the fluid. This phenomenon is known as *added mass* and represents an *inertial effect*, not an external load or a real additional mass. In fact, the added mass is not modeled as an extra load, but rather as a dedicated *added mass matrix* that is summed to the physical mass of the system within the dynamic model. This term appears in the product between mass and acceleration, modifying the overall mass matrix, which may *lose the property of being positive definite*, unlike conventional mass matrices. The added mass also affects other dynamic terms, such as *centripetal and Coriolis contributions*. It depends on the *geometry of the body* and on the *submerged configuration*, and must be explicitly modeled to correctly describe the vehicle's behavior in a fluid environment. So, it is not an additional load applied to the structure, but rather an *inertial phenomenon* that alters the system's dynamics.

b. The added mass effect is considered in underwater robotics since the density of the underwater robot is comparable to the density of the water. **TRUE.**
In underwater robotics, the *added mass effect* is considered because, unlike in aerial robotics, the density of the fluid is comparable to that of the robot's body, making the fluid's inertia a significant contribution. This effect cannot be neglected as it substantially alters the system's dynamics, directly influencing the calculation of the forces required to generate motion. For this reason, the added mass effect is explicitly included in the dynamic model of underwater vehicles. In contrast, in aerial robotics, the density of air is much lower than that of the robot's body, and the added mass effect is negligible.

c. The damping effect helps in the stability analysis. **TRUE.**
The damping effect in underwater robotics is directly related to the viscosity of the fluid, which generates resistive forces that oppose the motion of the vehicle. These forces, known as drag and lift forces, typically act at the center of mass of the body and are proportional to the relative velocity between the vehicle and the surrounding fluid. In particular, the drag force is aligned with the direction of relative motion, while the lift force is orthogonal to it. Both are dissipative forces and are modeled using a damping matrix, $\mathbf{D}_{RB}$, which is defined to be positive. This matrix is typically considered constant and is applied to the square of the relative velocity—meaning that damping increases with higher fluid motion. In the dynamic model of the vehicle, the damping effect plays a crucial role in stability analysis. As a mechanism of energy dissipation, damping tends to reduce oscillations and promotes convergence toward an equilibrium state. This facilitates system stabilization. Therefore, damping introduces a stabilizing action.

d. The Ocean current is usually considered as constant, and it is better to refer it with respect to the body frame. **FALSE**
The ocean current is usually modeled as constant and irrotational, but only when expressed in the world-fixed reference frame. This is because, in the world frame, the current can be considered time-invariant and spatially uniform, i.e., with zero acceleration:

$$\mathbf{v}_c = \begin{bmatrix} v_{c,x} & v_{c,y} & v_{c,z} & 0 & 0 & 0 \end{bmatrix}^\top \in \mathbb{R}^6, \quad \dot{\mathbf{v}}_c = \mathbf{0}_6$$

However, if the current were expressed in the body-fixed frame, which moves and rotates over time, the current would no longer appear constant but would instead vary, making the modeling more complex. For this reason, in the hydrodynamics of underwater vehicles, the ocean current

is typically referred to the world frame, where it can be treated as a contribution to the relative velocity between the body and the surrounding water, without introducing artificial accelerations. So, the statement is false because it is only correct to model the current as constant when it is expressed in the inertial world frame, not in the body-fixed frame.

3. Simulation and Analysis of Gait Dynamics in a Quadruped Robot

In this exercise, the MATLAB simulation environment is used to analyze the dynamic behavior of a quadruped robot. The task involves integrating the QP solver `qpSWIFT` within the `MAIN.m` file to activate the already implemented quadratic optimization. Additionally, it requires modifying key parameters such as the gait, desired velocity, and physical properties of the robot, including mass and friction coefficient. The goal is to observe how these changes affect the robot's dynamics through the analysis of the resulting plots.

3.a

In the context of this exercise, the quadratic programming solver `qpSWIFT` was used to efficiently solve the quadratic optimization problem. The solver, already implemented within the simulation folder, was integrated into the `MAIN.m` file to solve, at each iteration, a QP problem defined by a quadratic cost function and a set of linear equality and inequality constraints.All input matrices were converted into sparse format (`sparse`) to optimize computational performance. The output `zval` contains the optimal solution of the problem, which is used to update the robot's control input. The solver also returns two informational structures: `basic_infoeq`, which includes essential data such as the exit flag, number of iterations, initialization time, and solve time; and `adv_infoeq`, which provides advanced diagnostic information, including the objective function value, dual variables, computation times for KKT condition checking and factorization, and the primal slack variables.
The integration of `qpSWIFT` made it possible to solve the QP problem at each control step, enabling the generation of the optimal command that guides the robot along the desired trajectory while satisfying the dynamic and physical constraints of the system.

3.b

In the second part of the exercise, several key parameters were modified within the `MAIN.m` and `get_params.m` files in order to analyze their effect on the behavior of the quadruped robot. The default parameters include a desired velocity of 0.5 m/s, a total robot mass of 5.5 kg, and a unit friction coefficient. The subsequent simulations were carried out by varying these parameters, as well as the robot's gait, in order to evaluate how different configurations affect the dynamic balance, ground reaction forces, and trajectory tracking accuracy.

Bound Gait

In the comparison between the plots related to the Bound gait, minimal differences are observed between the default case and the modified one, in which only the mass parameter was changed, from $m = 5.5\,\text{kg}$ to $m = 4.8\,\text{kg}$. (In this case, the default parameters are $m = 5.5\,\text{kg}$, $v = 2\,\text{m/s}$, and $\mu = 1$.) In the position plot, in both cases an acceptable tracking is observed, with a slight deviation along the x-axis. The final extension along the x-axis is also substantially identical, since the desired velocity was not modified. In the velocity plot, it is noted that the v_x component in the modified case reaches slightly lower peak values compared to the default case: the oscillations remain regular, but the crests are less pronounced. This is consistent with the reduction in mass, which slightly reduces the intensity of the system's dynamic response. The v_z component shows a similar behavior, with slightly attenuated oscillations in the modified case. Regarding angular velocity, only the ω_y component is present in both cases. This is plausible because the Bound gait is symmetric with respect to the sagittal plane, and the robot's body primarily oscillates

forward and backward around the y-axis. The two configurations show very similar profiles in both amplitude and frequency. Finally, in the plot of the vertical ground reaction force F_z, a difference is observed: in the modified case, the peaks are slightly lower, consistently with the mass reduction, which results in a lower ground reaction force for each leg.
So, the overall profile remains similar in both simulations, with limited variations in vertical force F_z and velocity.

Result with default parameters

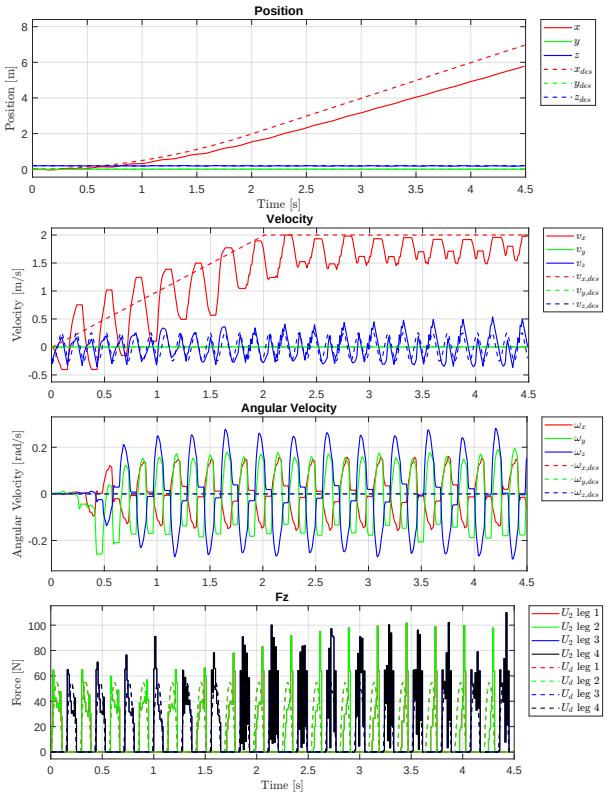

Result with modified parameters

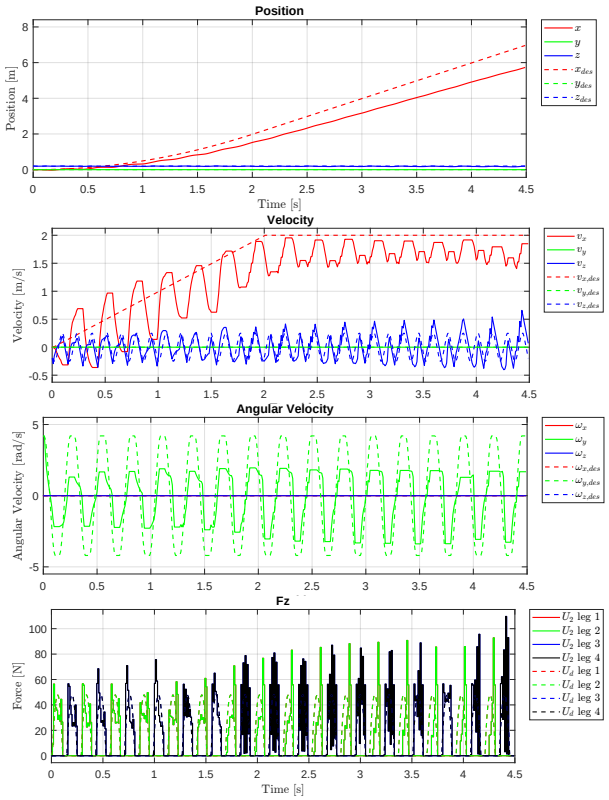

In another test, it was observed that, while keeping all other default parameters unchanged and critically reducing the friction coefficient from the default value $\mu = 1$ to the modified value $\mu = 0.4$, the system becomes unstable and the robot falls. This behavior is due to insufficient ground adherence: with such a low friction coefficient, the contact forces are no longer sufficient to generate the necessary ground reaction forces to maintain stability during the stance phases. In fact, the test showed that the trajectory along the x-axis initially follows the desired one, but then deviates significantly, becoming chaotic as the robot loses balance. Regarding velocity, it was noted that the v_x component exceeds the desired value and no longer stabilizes around the reference, but begins to oscillate increasingly, indicating a loss of control. Overall, the system can no longer regulate either the translational or rotational motion, and the robot collapses due to the reduced ability to generate sufficient friction forces to stabilize itself.

Gallop Gait

In the context of the Gallop gait, the modification of the kinematic and physical parameters of the robot, from the default values to the modified ones $v = 0.8\,\mathrm{m/s}$, $m = 4.6\,\mathrm{kg}$, $\mu = 1.2$, resulted in variations in the trajectory, as observed in the comparison of the plots. In the modified case, the x-component of the position grows with a steeper slope, consistent with the increase in the desired velocity, reaching nearly twice the distance traveled compared to the default case. This confirms that the system was indeed able to follow a faster gait. The y and z components remain overall stable in both cases, without significant deviations. Therefore, the parameter modification produced an improvement in performance in terms of velocity and distance traveled, with tracking

still effective. In the comparison of the velocity plots, both cases show an oscillatory profile, typical of the Gallop gait. In the modified case, the average value of the v_x component is higher, consistent with the increased desired velocity. The v_y and v_z components show similar amplitude in both cases, but appear slightly reduced in the modified case. Regarding angular velocity, the ω_y component in the default case shows greater amplitudes on both sides of the axis, reaching more pronounced positive and negative peaks. With the modified parameters, ω_y is overall more attenuated, particularly after the initial phase of the simulation. This behavior is attributable to greater lateral stability of the system, ensured by the reduced mass and the increased friction coefficient, which provides better ground adherence. The ω_x component remains substantially unchanged in both cases. As for ω_z, a reduction in amplitude is observed in the modified case, with more limited oscillations, probably due to the higher friction that limits rotation around the vertical axis. In the comparison of the vertical ground reaction force F_z, a generally similar dynamic is observed in both cases, but with a clear difference in the amplitude of the peaks. In the modified case, the forces exerted by the legs are more contained: the peaks are lower than those in the default case, where the robot's mass was greater. The reduction in mass therefore results in lower ground reaction forces, given the same step dynamics. No relevant variations in the frequency or regularity of the impulses are detected, which remain cyclic and well distributed over time. The slight reduction in force intensity may also be due to the increased desired velocity, which reduces ground contact time and leads to shorter but quicker thrusts.

Result with default parameters

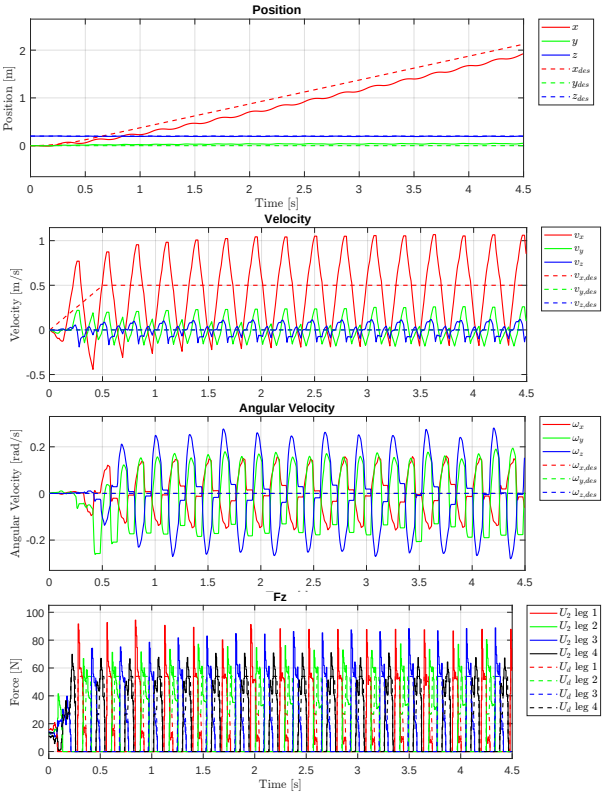

Result with modified parameters

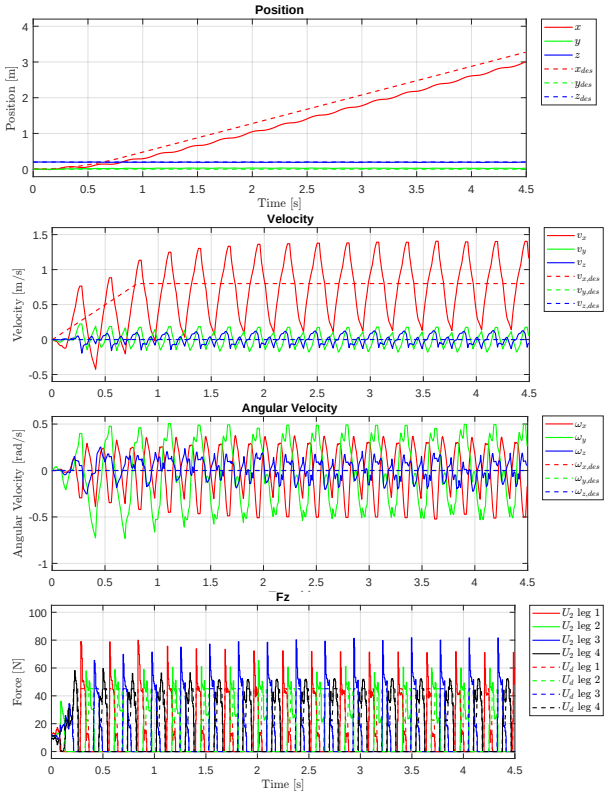

Trot-Run Gait

In the comparison between the position plots for the Trot-Run gait, it is observed that the modification of the kinematic and physical parameters of the robot (with increased speed to $v = 0.9\,\mathrm{m/s}$, reduced mass to $m = 5.2\,\mathrm{kg}$, and friction coefficient set to $\mu = 0.8$) results in a clear increase in the distance traveled along the x-axis, as expected. The x component shows a steeper slope, indicating a faster progression, and reaches final values significantly higher than in the default case. However, the actual trajectory deviates slightly more from the desired one compared to the default case: tracking remains accurate nonetheless. The y and z components, on the other hand,

remain almost perfectly aligned with their desired counterparts in both cases, indicating that transverse and vertical stability have not been compromised by the modifications.In the comparison between the velocity plots for the Trot-Run gait, marked differences are observed between the two cases. For the v_x component, in the modified case the actual velocity quickly stabilizes after a brief transient and closely follows the desired velocity, with minimal oscillations. In contrast, in the default case, v_x exhibits a consistently wavy trend around the desired value, with regular oscillations persisting throughout the simulation. The v_y component in the default case shows low-amplitude oscillations, while in the modified case the oscillations are visibly more frequent and larger, indicating greater lateral activity due to the more energetic dynamics of the gait at higher speed and lower friction. In fact, the reduced friction coefficient may require greater lateral adjustments to maintain stability. The v_z component is almost null in the default case, with the signal remaining close to zero and near the desired profile. In the modified case, however, regular and clearly visible vertical oscillations appear, indicating a more pronounced movement along the vertical axis. This behavior is consistent with the increased speed and reduced friction, which enhance the rhythmic lifting and lowering of the body during stepping, reflecting a more pronounced vertical dynamic. For the angular velocity plots, significant differences are observed between the default and modified parameter cases. For the ω_x component, the oscillations maintain a similar amplitude in both cases, with a regular sinusoidal shape, indicating that the dynamics around the sagittal axis remain nearly unchanged. The ω_y component shows a clear change in oscillation shape. In the default case, the signal exhibits a smoother and more continuous trend, with a rounded triangular shape, indicating gradual transitions between positive and negative peaks. In the modified case, however, the oscillation takes on a more trapezoidal shape, characterized by nearly flat segments at the peaks and more abrupt transitions between phases. This indicates a more impulsive and decisive behavior, due to the higher speed and lower friction, which lead to quicker and segmented corrections of the robot's lateral posture. The ω_z component shows the most pronounced difference: in the default case, the oscillations are of low amplitude and follow the desired reference more closely, whereas in the modified case, the signal deviates more from the desired trajectory, with large oscillations that reflect a more intense rotational dynamic around the vertical axis, caused by the increased effort required to maintain directional stability with reduced friction. Regarding the vertical force F_z plots, in the modified configuration the force impulses are more frequent and sharper, characterized by a narrow and vertical profile indicating shorter but more intense contact phases. This greater impulsivity suggests a more dynamic and reactive locomotion, consistent with the higher desired speed. Additionally, the increased frequency of impulses indicates an accelerated gait cycle. In contrast, in the default case, the force signals show a more distributed trend over time, with less sharp peaks, indicative of a more regular and controlled walk, consistent with a slower gait and higher friction coefficient. Overall, the system with modified parameters exhibits a more energetic behavior, but also more "impactful," as the forces are concentrated in shorter moments, potentially increasing mechanical stress.

Result with default parameters

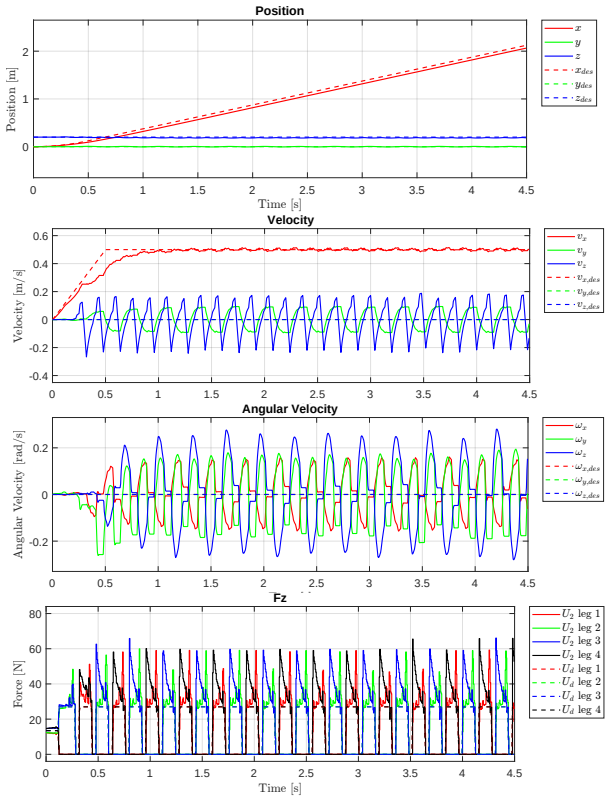

Result with modified parameters

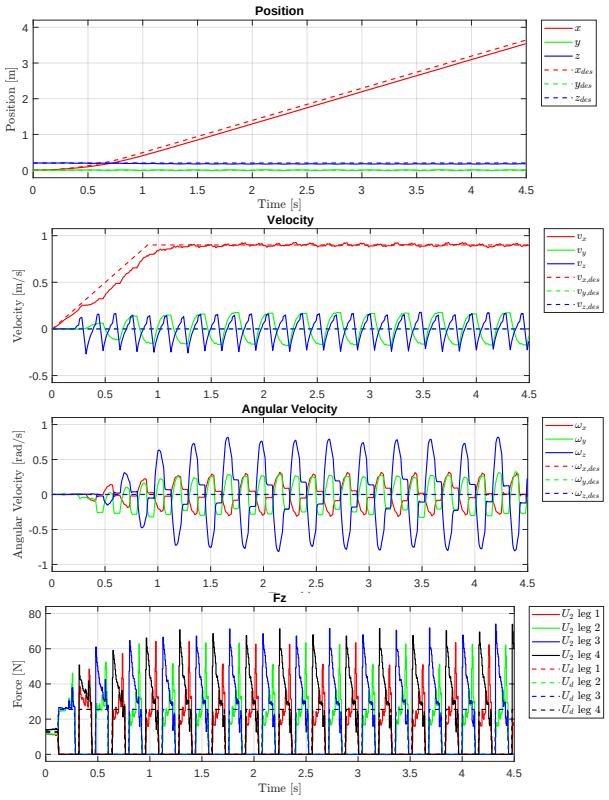

Crawl Gait

In the comparison between the position plots for the Crawl gait, the effect of modifying the robot's kinematic and physical parameters — with desired velocity reduced to $v = 0.37\,\text{m/s}$, mass increased to $m = 6.1\,\text{kg}$, and friction coefficient increased to $\mu = 1.2$ — is mainly reflected in the behavior along the x-axis. In the default case, the trajectory along x shows a steeper slope and reaches higher final values, consistent with the higher desired velocity. Conversely, in the modified case, the x-curve grows more slowly and ends at a shorter distance, as expected. The y and z components, on the other hand, remain substantially overlapped with their respective desired references in both cases. As for the velocity plots, all three signals v_x, v_y, and v_z show a qualitatively similar trend in both cases, characterized by regular periodic oscillations. However, in the modified case, a general decrease in the maximum values reached can be observed, consistent with the lower desired velocity. In particular, v_x shows a lower average value, while the v_y and v_z components maintain similar but slightly reduced amplitudes. This reflects a slower and less energetic dynamic, due to the combination of increased mass (which reduces the system's responsiveness) and higher friction (which stabilizes but damps the movement). In the comparison between the plots related to the Crawl gait, no significant differences emerge in the angular velocity profiles or in the vertical force F_z plots. The angular velocity components ω_x, ω_y, and ω_z maintain almost unchanged amplitude in both cases, with regular and symmetrical oscillations that do not show appreciable variations in frequency or shape. Their adherence to the desired profile also remains stable, suggesting that the changes made to the physical and kinematic parameters did not have significant effects on the robot's body rotational dynamics. Similarly, in the comparison between the vertical force F_z plots for the four legs, an almost identical behavior is observed between the two cases. The system maintains stable and regular performance even after the parameter changes, probably because this slower and more controlled gait is inherently less sensitive to small variations in dynamic and kinematic values.

Result with default parameters

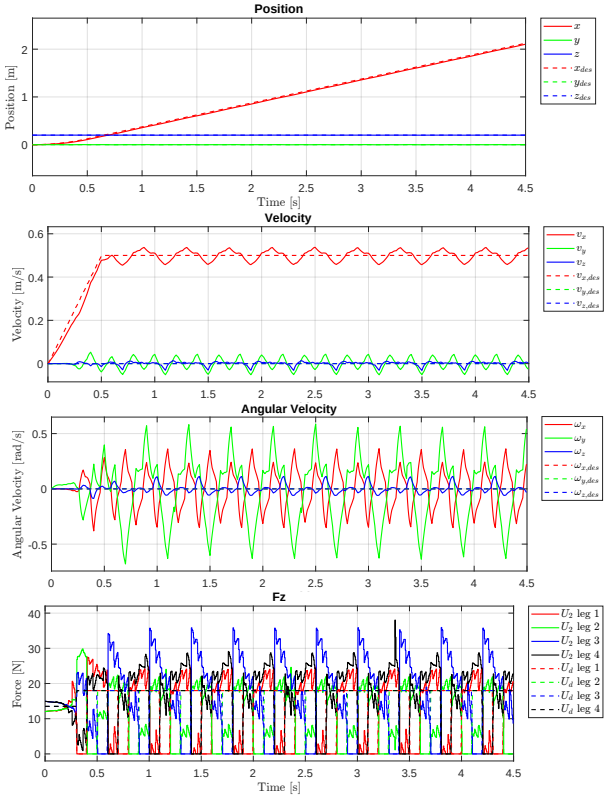

Result with modified parameters

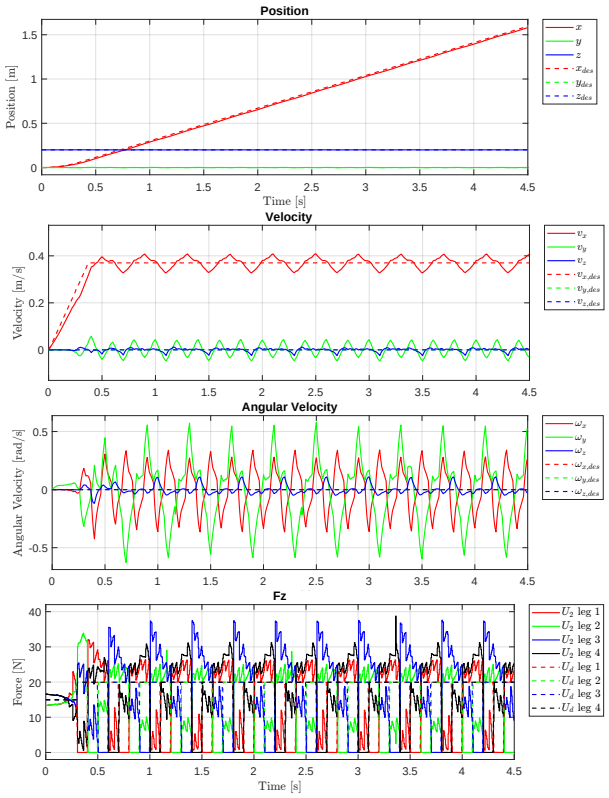

Trot Gait

Following the modification of the robot's kinematic and physical parameters — namely an increase in the desired velocity, and a reduction in mass and friction coefficient — some differences can be observed in the plots resulting from the two simulations. Specifically, the parameters were changed from the default values: desired velocity $v = 0.5\,\text{m/s}$, mass $m = 5.5\,\text{kg}$, friction coefficient $\mu = 1.0$, to the modified values: $v = 0.7\,\text{m/s}$, $m = 5.0\,\text{kg}$, $\mu = 0.7$.

In the position plot, the tracking of the desired trajectory remains accurate, with minimal deviations between the actual and reference trajectories, although slightly more pronounced compared to the default case. As expected, the increase in desired velocity in the modified case results in a greater distance traveled along the x-axis.

Regarding the velocity plot, it is observed that the v_x component correctly reaches a higher average value in the second case, stabilizing around $0.7\,\text{m/s}$. The initial transient phase is slightly slower compared to the default case, but once the desired velocity is reached, the behavior is regular and free of significant additional oscillations. The v_y and v_z components do not show substantial variations, maintaining similar behavior in both simulations.

In the angular velocity plot, more evident differences are observed: in the modified case, the oscillations are slightly more pronounced. This behavior can be attributed to the reduction in mass and friction coefficient, which make the system less damped. However, the angular error remains limited.

Finally, in the plot of the vertical component of the ground reaction forces F_z, the overall trend is similar between the two simulations. However, in the default case, slightly more pronounced peaks are observed compared to the modified case. This behavior is attributable to the greater mass of the robot in the initial configuration, which results in higher ground reaction forces. The mass reduction in the modified case instead leads to a lighter load on each leg, with a consequent decrease in the intensity of the vertical force peaks.

The parameter modification increased the desired velocity without introducing major instabilities, but it did result in a slight amplification of angular oscillations and more pronounced deviations in tracking, although still very limited.

Result with default parameters

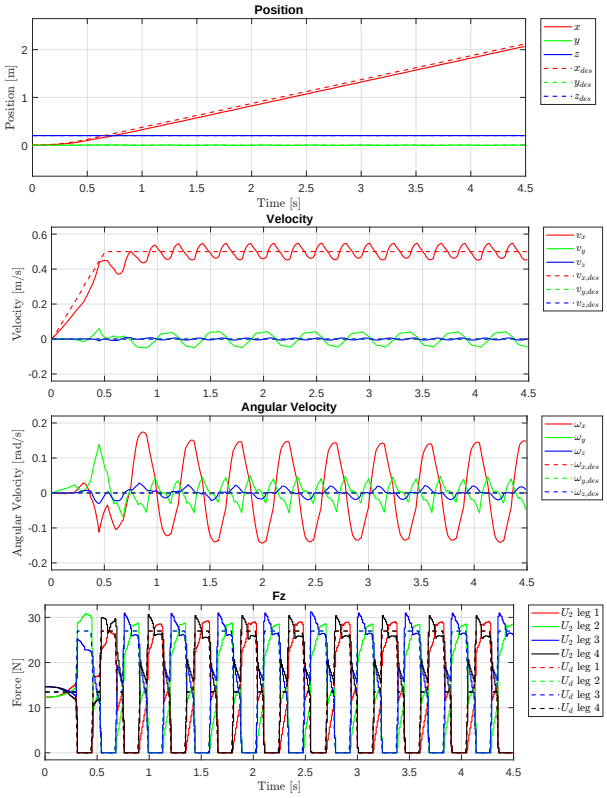

Result with modified parameters

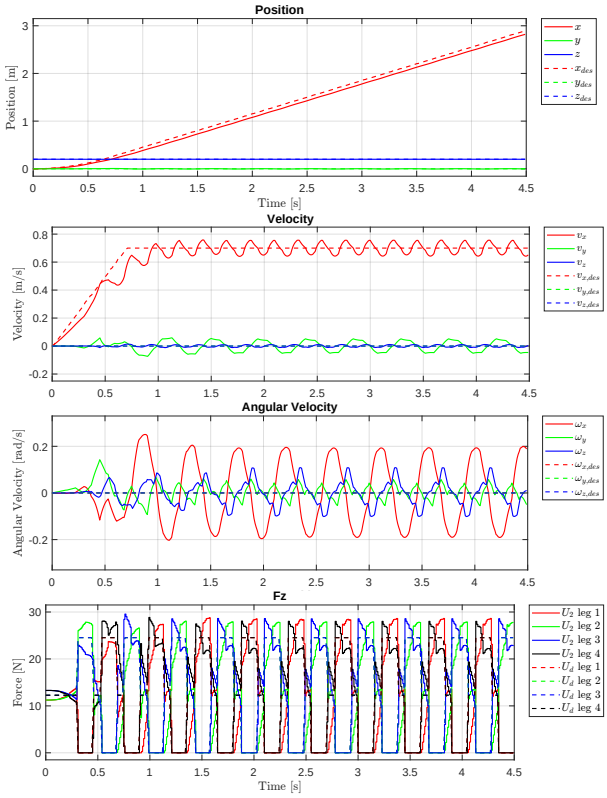

Further tests showed that, while keeping all other default parameters unchanged and significantly increasing the desired velocity from $v = 0.5\,\text{m/s}$ to $v = 5.0\,\text{m/s}$, the system becomes unstable and the robot exhibits an abnormal gait, far from the expected Trot pattern. In particular, the v_x component consistently exceeds the desired value and continues to increase without stabilizing: the system fails to control the acceleration along the main direction. Meanwhile, all angular velocity components display growing and chaotic oscillations: the amplitudes become increasingly larger over time. At a speed of $5.0\,\text{m/s}$, the stance time of the legs is drastically reduced, and the system no longer has enough time to properly complete the support phase. The robot loses coordination, is no longer able to regulate the gait, and develops an irregular behavior that results in a complete loss of stability.

Pacing Gait

In the comparison between the position plots for the Pacing gait, the modification of the robot's kinematic and physical parameters (desired velocity increased to $v = 0.7\,\text{m/s}$, mass reduced to $m = 4.4\,\text{kg}$, and friction coefficient increased to $\mu = 1.4$) results in an increased distance traveled along the x-axis, as expected. In both cases, trajectory tracking is accurate. The y and z components remain almost superimposed on the desired references in both configurations. As for the velocity plots, the v_x component in both cases exhibits regular oscillation around the desired value, but with a higher oscillation center in the modified case (around $0.7\,\text{m/s}$ compared to $0.5\,\text{m/s}$ in the default case). The oscillation shape is similar, but with a slight steepening of the rising edges in the modified case, indicating more responsive control. The v_y component, in both cases, shows an approximately triangular periodic pattern, but with reduced amplitude in the modified case. This suggests a slightly more restrained lateral dynamic, likely favored by the increased friction coefficient that stabilizes lateral behavior. The v_z component remains similar in both cases, with regular low-amplitude oscillations. The angular velocities ω_x, ω_y, and ω_z show an almost identical trend in both cases. The profiles maintain the same frequency and morphology,

with regular, symmetric, and well-distributed oscillations. The only slight difference observed is a minimal reduction in oscillation amplitude in the case with modified parameters, suggesting a slightly less energetic dynamic, consistent with the lower mass that reduces rotational inertia. In the comparison between the vertical force F_z plots, it is observed that in the modified case, all force peaks are systematically lower than in the default case. This behavior is consistent with the reduction in the robot's mass: a lower mass implies lower ground reaction forces under the same gait dynamics. Despite the increase in friction coefficient and desired velocity, which make the gait more responsive and potentially more impulsive, the vertical force values decrease precisely due to the lower mass.

Result with default parameters

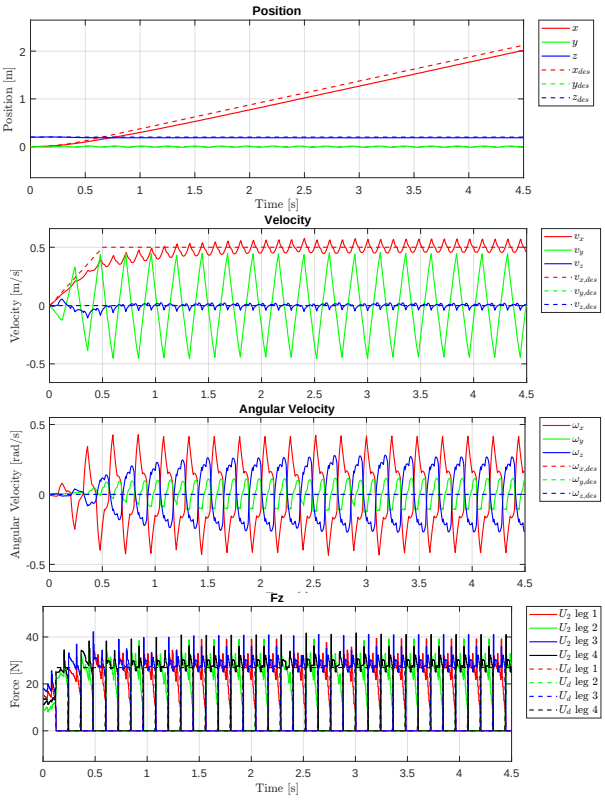

Result with modified parameters

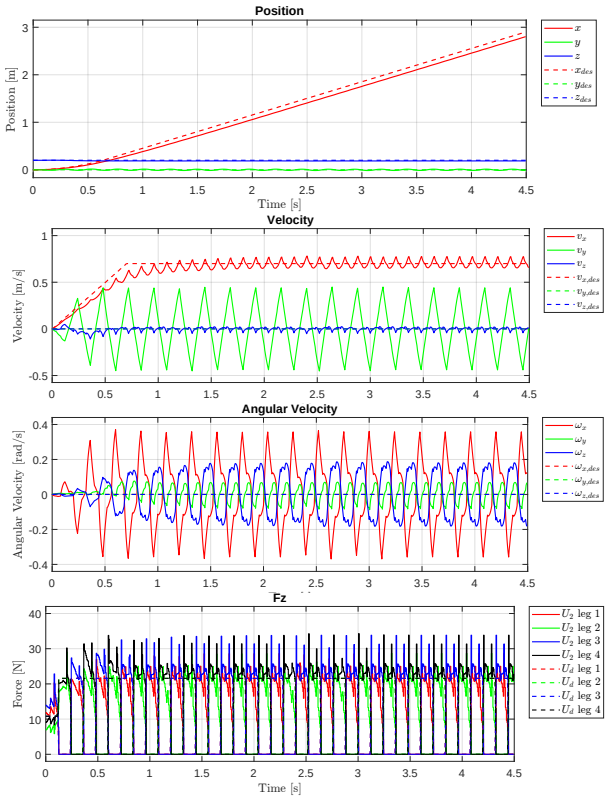

4. Dynamic Analysis of the Rimless Wheel

The objective of this exercise is to analyze the **dynamic behavior of the rimless wheel**, one of the simplest and most effective models for describing **passive walking**.This model, which is completely passive and actuator-free, moves solely due to **gravity** and its own **geometric structure**. It consists of a set of **rigid legs** arranged radially around a central point representing the hip, with a **point mass** concentrated at that location. During motion, only **one leg at a time** is in contact with the ground; this leg is considered to be in the *stance phase*, and its motion represents a walking step. Among the main modeling assumptions, the following are considered:

- Collisions with the ground are **impulsive and inelastic**, preserving only the **angular momentum** about the point of impact.
- The stance foot behaves as a **hinged joint** and does not slip, satisfying a **holonomic constraint**.
- The **transition** from one leg to the next is **instantaneous**, meaning that there is **no double support phase**.

The system moves on an **inclined plane** with angle γ relative to the horizontal. The angle between two consecutive legs is 2α, and each leg has length $l > 0$. The parameters must satisfy

the conditions:

$$0 \leq \gamma < \frac{\pi}{2}, \quad 0 < \alpha < \frac{\pi}{2}$$

During the stance phase, the system evolves dynamically like a **simple pendulum** with a shifted angular origin. Its equation of motion is:

$$\ddot{\theta} = \frac{g}{l} \sin(\theta)$$

where θ is the angle between the stance leg and the vertical, and g is the gravitational acceleration. An **impact with the ground**, marking the transition to the next leg, occurs when:

$$\theta = \gamma \pm \alpha$$

i.e., when the angle of the stance leg reaches a threshold determined by the geometry and the slope of the plane. In order for the system to actually begin walking, the **angular velocity immediately after impact**, $\dot{\theta}(0^+)$, must exceed a **minimum threshold**:

$$\omega_1 = \sqrt{\frac{2g}{l}(1 - \cos(\gamma - \alpha))}$$

This threshold ensures that the **central mass has sufficient kinetic energy** to overcome the potential barrier imposed by the new stance leg. If this condition is not met, the motion comes to a stop; otherwise, the system can quickly **converge to a stable limit cycle**, that is, a periodic solution representing a regular passive gait.

4.a

In the file `rimless_wheel.m`, the initial angular velocity $\dot{\theta}_0$ was modified, exploring different cases, in order to analyze: the behavior of the state variables over time; the evolution in the phase plane; the presence of equilibria or limit cycles; and their respective basins of attraction. The minimum kinetic threshold necessary for the system to start walking passively, defined by the formula of ω_1, was taken into account. In the context of the exercise, with the default parameters (leg length $l = 1\,\text{m}$, $\gamma = 0.08\,\text{rad}$, and $\alpha = \pi/8$), this threshold turns out to be $\omega_1 \approx 0.97\,\text{rad/s}$.
Case 1 – $\dot{\theta}_0 = 1.2 > \omega_1$ The system starts with an initial angular velocity higher than the minimum threshold, therefore with sufficient energy. As shown in the graph, the temporal evolution of the state variables $\theta(t)$ and $\dot{\theta}(t)$ displays a clearly periodic behavior, indicating a stable limit cycle. In the phase portrait, it can be seen that the orbits converge toward a closed trajectory: this confirms that the system quickly enters a limit cycle, which represents a regular and stable passive gait. The initial point falls within the basin of attraction of this limit cycle, and the resulting behavior is that of a cyclic attractor.

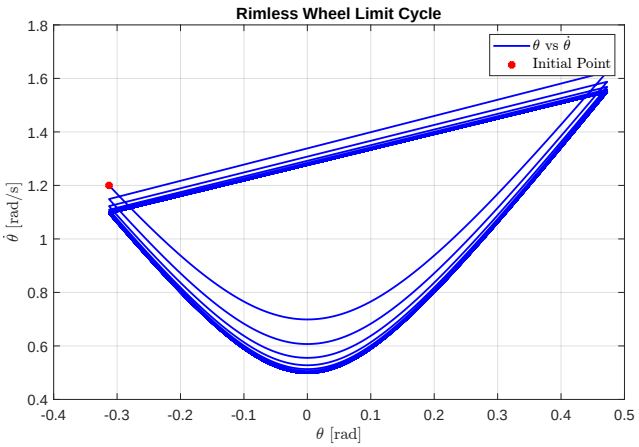

Figure 1: Rimless Phase

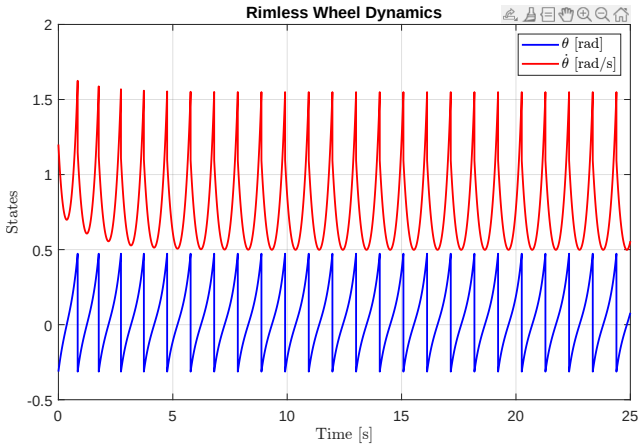

Figure 2: Rimless Time

Case 2 – $\dot{\theta}_0 = 0.93 < \omega_1$ In this case, the initial angular velocity is lower than the minimum threshold, and therefore insufficient to initiate a stable passive walk. As shown in the graph, after a few initial steps, the temporal evolution of the state variables shows a progressive decay: $\theta(t)$ tends to a constant value, while $\dot{\theta}(t)$ quickly converges to zero. The system comes to a stop, lacking sufficient kinetic energy to overcome the constraint imposed by the stance leg. In the phase portrait, the orbits show a clear convergence towards a fixed point, indicating the achievement of a static equilibrium condition. This fixed point represents a stable attractor, distinct from the limit cycle observed in the previous case. The overall behavior observed demonstrates the coexistence of two attractors in the system: a limit cycle, reached only if the initial energy is sufficient, and a fixed point, towards which the system converges otherwise. Therefore, the basin of attraction depends critically on the initial condition $\dot{\theta}_0$.

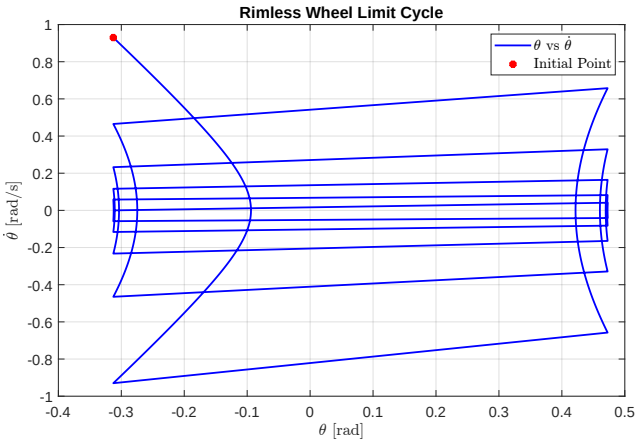

Figure 3: Rimless Phase

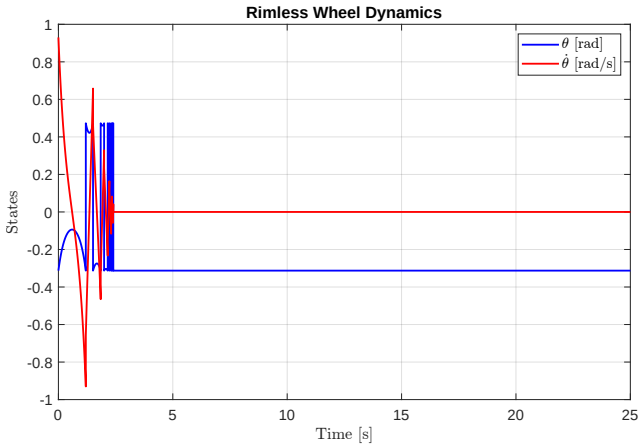

Figure 4: Rimless Time

Case 3 – $\dot{\theta}_0 = -2.0 < 0$ In this case, the initial angular velocity is negative, that is, oriented in the opposite direction to that expected for passive walking. As shown in the graph, the system initially exhibits a complex and irregular dynamic, but after a few seconds$\dot{\theta}(t)$ vanishes, indicating the complete stop of the motion. Also in the phase portrait, the evolution of the orbits shows a rapid convergence towards a fixed point, similar to the cases with insufficient initial velocity. No limit cycle is observed, and the system does not walk backward, confirming that the initial energy is not only insufficient, but also incompatible with the natural direction of passive motion. This trajectory also falls within the basin of attraction of the static equilibrium, demonstrating that this attractor also includes initial conditions with retrograde velocity.

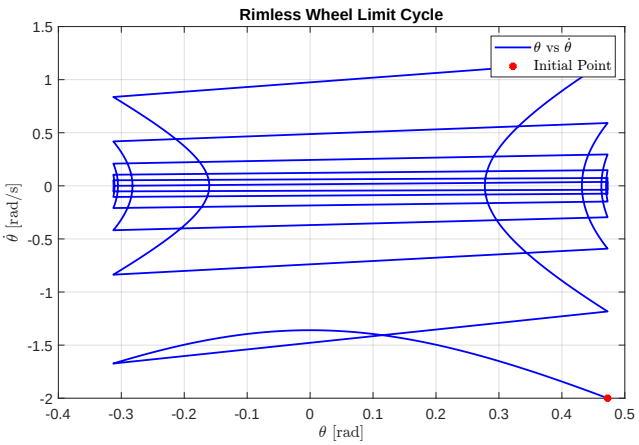

Figure 5: Rimless Phase

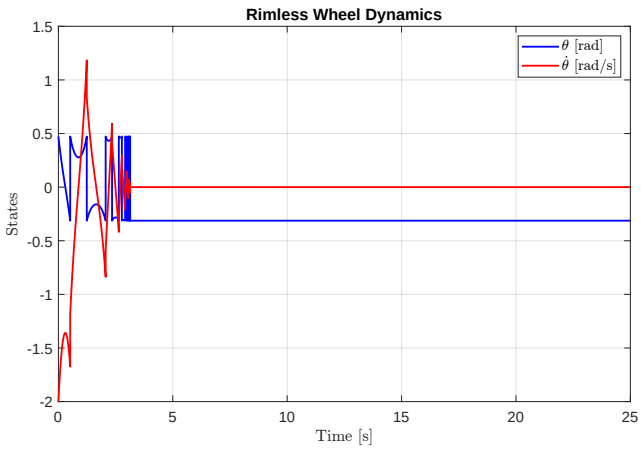

Figure 6: Rimless Time

From the analysis carried out, it is observed that the system converges to two distinct equilibria, depending on the initial condition:

- **Static equilibrium:** the system converges to this state when the initial angular velocity $\dot{\theta}_0$ is lower than the threshold ω_1, or is negative. In both cases, the initial energy is not sufficient (or is directed in the opposite sense) to sustain the motion, and the system stops after a few steps. This equilibrium represents a state of immobility and constitutes a stable attractor.

- **Stable limit cycle:** the system converges to a stable periodic motion when $\dot{\theta}_0 > \omega_1$. In this case, the initial velocity provides sufficient kinetic energy to maintain the step, and the system quickly reaches a regular passive gait. This limit cycle represents a second attractor of the system.

There are therefore two distinct attractors: a fixed point and a limit cycle. Their respective basins of attraction are separated by the threshold ω_1: initial conditions with $\dot{\theta}_0 > \omega_1$ fall within the basin of the limit cycle, while those with $\dot{\theta}_0 \leq \omega_1$ (including negative values) fall within the basin of the static equilibrium.

4.b

The ability of the system to walk passively depends on the critical value ω_1, which is a function of the physical parameters l, γ, and α. In this phase of the analysis, the initial angular velocity $\dot{\theta}_0 = 0.95\,\text{rad/s}$ is kept constant, while the three parameters are varied to evaluate their impact on the system's behavior. An increase in l leads to a decrease in ω_1, making walking easier. Similarly, an increase in γ enhances the gravitational component that drives the motion, also lowering ω_1 and favoring the attainment of the limit cycle. An increase in α also results in a reduction of ω_1, but its effect on the dynamics is not always positive: excessively large angles produce wider steps, which can make contact with the next leg more difficult. Conversely, very small values of α increase the threshold ω_1 and require more initial energy to sustain motion. Finally, if $\gamma > \alpha$, there is a risk of exceeding the static stability limit: the central mass would always lie beyond the contact point with the ground, preventing the existence of a stable equilibrium.
Case 1 – $l = 0.8$, $\alpha = \pi/6$, $\gamma = 0.05$ In this configuration, the system does not enter a limit cycle but stops quickly. As shown in the graph on the left, both $\theta(t)$ and $\dot{\theta}(t)$ rapidly decay to constant values, indicating the absence of cyclic motion. In the phase portrait on the right, the orbits do not converge toward a closed trajectory but rapidly contract toward a fixed point. The reason is related to the fact that, with these parameters, the critical value ω_1 is greater than $0.95\,\text{rad/s}$. In particular: The reduced slope $\gamma = 0.05\,\text{rad}$ does not provide enough potential energy to trigger passive walking; The inter-leg angle $\alpha = \pi/6$ is relatively large, so the next leg is distant, and with the available initial energy the system fails to reach it. As a result, the system behaves as if the initial condition falls within the basin of attraction of the static equilibrium, and comes to a stop.

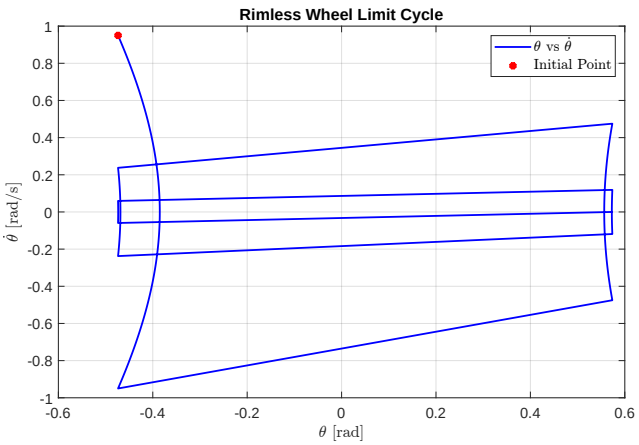

Figure 7: Rimless Phase

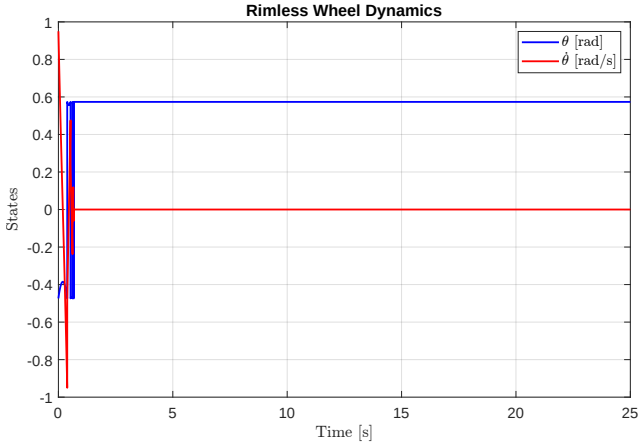

Figure 8: Rimless Time

Case 2 – $l = 0.8$, $\alpha = \pi/12$, $\gamma = 0.05$ Compared to the previous case (where $\alpha = \pi/6$), only one parameter has been changed: the angle α, reduced from $\pi/6$ to $\pi/12$, while keeping $l = 0.8$ and $\gamma = 0.05$ unchanged. The graphs clearly show that, unlike the previous case in which the system stopped, the wheel now enters a stable limit cycle. The graph on the left highlights the time evolution of the state variables: $\theta(t)$ and $\dot{\theta}(t)$ show periodic behavior after an initial transient phase, indicating the onset of regular passive walking. The graph on the right confirms this result: the orbits in the phase plane $(\theta, \dot{\theta})$ clearly converge towards a closed trajectory, which represents an attractive limit cycle. Reducing α decreased the distance between the legs: this implies that the next leg is closer and thus more easily reachable with the same initial energy. It also modified the threshold ω_1, increasing it. Even though ω_1 increased, the shorter distance to the next leg and the higher step frequency made the use of the available energy more efficient. The change of a single parameter, α, was sufficient to switch from a system that stopped to one that walks passively in a stable manner. This highlights that passive walking depends not only on the comparison between $\dot{\theta}_0$ and ω_1, but also on the geometric configuration, which influences the overall dynamic efficiency.

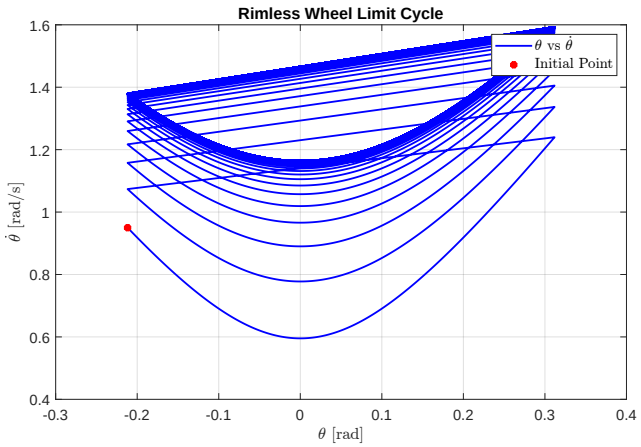

Figure 9: Rimless Phase

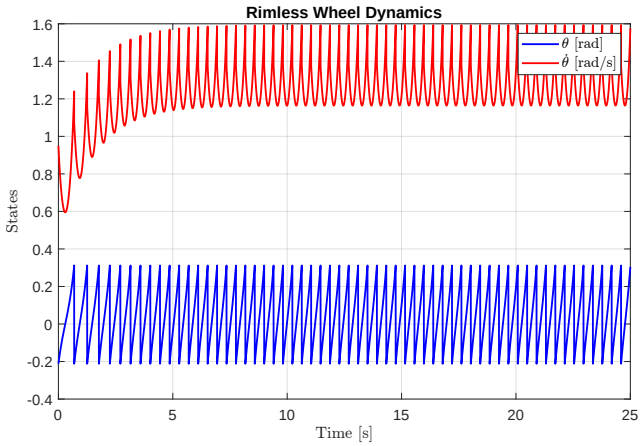

Figure 10: Rimless Time

Case 3 – $l = 1.2$, $\alpha = \pi/10$, $\gamma = 0.15$ In this configuration, the system quickly converges to a stable and wide limit cycle, as evident both in the time-domain graph and in the phase portrait. The evolution of $\theta(t)$ and $\dot{\theta}(t)$ shows a regular periodic behavior with significantly higher velocity values compared to the previous cases. The orbits in the phase plane clearly converge towards a closed trajectory with large amplitude. This dynamic is mainly due to the increase in slope $\gamma = 0.15$, which provides more potential energy and facilitates exceeding the threshold ω_1, even with $\dot{\theta}_0 = 0.95$. Additionally, the greater leg length $l = 1.2$ further reduces ω_1, making the system more prone to passive walking, which in this case is faster and more energetic.

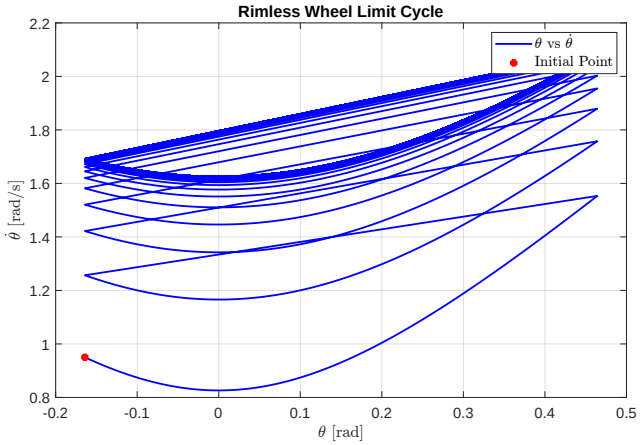

Figure 11: Rimless Phase

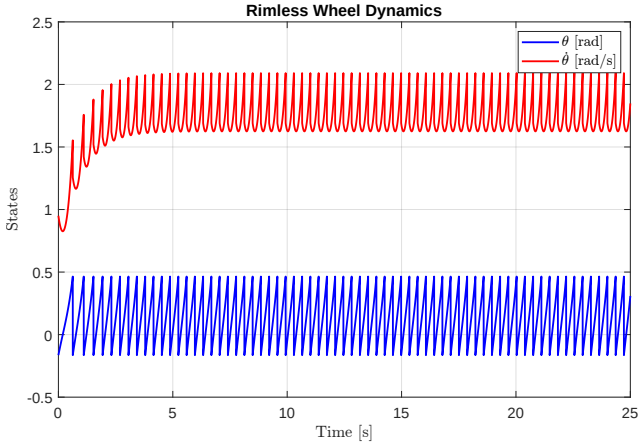

Figure 12: Rimless Time

The analysis conducted on the three cases, while keeping the initial angular velocity $\dot{\theta}_0 = 0.95\,\text{rad/s}$ constant, highlighted how variations in the physical parameters of the system — leg length l, inter-leg angle α, and ground inclination γ ,directly influence the equilibrium conditions of the rimless wheel. These parameters determine the critical threshold ω_1, above which the system can initiate and sustain stable passive walking. In the first case, with unfavorable initial parameters, the system quickly stops, falling into the basin of static equilibrium. In the subsequent cases, by modifying only one of the parameters, reducing α, or increasing γ and l, it is possible to overcome the required energy threshold and trigger a stable limit cycle. This demonstrates that even a single change can significantly alter the system's dynamics, leading to different equilibrium conditions. Furthermore, parameter changes do not only determine the presence of a limit cycle, but also affect its shape and dynamic characteristics: the step amplitude, the frequency, and the angular velocity reached in steady-state. Therefore, it can be concluded that the three physical parameters of the system not only determine the achievement of cyclic equilibrium, but substantially shape the quality and efficiency of the resulting passive motion.